Discrete dislocation modelling of submicron indentation

Widjaja, A; Van der Giessen, E; Needleman, A

Published in:
Materials science and engineering a-Structural materials properties microstructure and processing

DOI:
10.1016/j.msea.2005.01.074

Publication date:
2005

Materials Science and Engineering A 400–401 (2005) 456–459

www.elsevier.com/locate/msea

Discrete dislocation modelling of submicron indentation

Andreas Widjaja[a], Erik Van der Giessen[a,*], Alan Needleman[b]

[a] *University of Groningen, Department of Applied Physics, Nyenborgh 4, 9747 AG Groningen, The Netherlands*

[b] *Brown University, Division of Engineering, Providence, RI 02912, USA*

Received 13 September 2004; received in revised form 14 December 2004; accepted 3 January 2005

Abstract

Indentation of a planar single crystal by a circular rigid indenter is analyzed using discrete dislocation plasticity. The crystal has three slip systems and is initially dislocation-free, but edge dislocations can nucleate from point sources inside the crystal. The lattice resistance to dislocation motion, the interaction with point obstacles and dislocation annihilation are incorporated through a set of constitutive rules. Indentation is displacement driven and at each stage of the loading history, a boundary-value problem is solved for the evolution of the indentation pressure and the contact size. Preliminary results are presented for various values of the density of dislocation sources.

Keywords: Discrete dislocations; Nanoindentation; Size effects

1. Introduction

Indentation at the micro- and nano-scale can reveal a distinct size effect, e.g. [1,2], whereas in continuum plasticity the indentation hardness is scale independent. A variety of analyses have been carried out using atomistics, dislocation dynamics and strain gradient plasticity to model this size dependence, see e.g. [3–7]. At a sufficiently small scale, the size of the region of high stress under the indenter is generally less than the defect spacing, so that the hardness is set by the condition governing dislocation nucleation in a perfect crystal. At the (sub-)micrometer scale, which is considered here, the size of the high stress region is large enough to encompass internal dislocation sources, but small enough for the discreteness of dislocations to play a role.

Indentation is a complex, mixed traction-displacement boundary-value problem. Previous discrete dislocation simulations, [5,7], have employed special approximations to simplify the indentation problem. Here we use the versatile superposition framework of [8] to solve the boundary-value problem for depth-driven indentation.

2. Model

We perform small-strain discrete dislocation calculations of two-dimensional, plane strain indentation of a single crystal by a circular rigid indenter. The crystal is assumed to be symmetric relative to the x_2-axis of indentation and to have three slip systems oriented at 30°, 90° and 150° from the free x_1–x_2-surface, as shown in Fig. 1(a). This approximates a (1 1 0) projection of an FCC crystal with the [0 0 1]-direction parallel to the x_1-axis.

Plastic deformation is described in terms of the generation and glide of edge dislocations on these slip planes, according to a set of constitutive rules outlined in [8]. The material is taken to be free of dislocations initially, but contains an initial distribution of dislocation sources and point obstacles. The sources are a 2D representation of Frank–Read sources, and the obstacles model forest dislocations, both of which are

* Corresponding author. Tel.: +31 50 3638046; fax: +31 50 3634886.
E-mail address: E.van.der.Giessen@rug.nl (E. Van der Giessen).

0921-5093/$ – see front matter © 2005 Elsevier B.V. All rights reserved.
doi:10.1016/j.msea.2005.01.074

regarded as being present due to pre-existing dislocations. Cross slip and climb are not considered, and glide is governed by a linear drag relation.

To calculate the fields in the indented material containing a distribution of dislocations, we use the known singular solution of an edge dislocation in infinite space and adopt superposition [8] to correct for the actual boundary conditions. This involves the computation of image stress fields which we do by the finite element method.

Because of symmetry only half of the problem, i.e. for $x_1 \geq 0$, is analyzed. Indentation is implemented by incrementally prescribing the displacements according to the indenter shape over the current contact length. The indentation force per unit out-of-plane thickness, F, is calculated from the resulting tractions along the indenter, while the rest of the surface of the crystal, $x_2 = 0$, is left traction free. Dislocations may leave the crystal through the free surface, thus leaving a surface step. The contact length a is continuously updated during the calculation, on the basis of the highly refined mesh near the surface of contact, as shown in Fig. 1(b). After each increment of indentation, the dislocation structure is updated as are the stress and displacement fields.

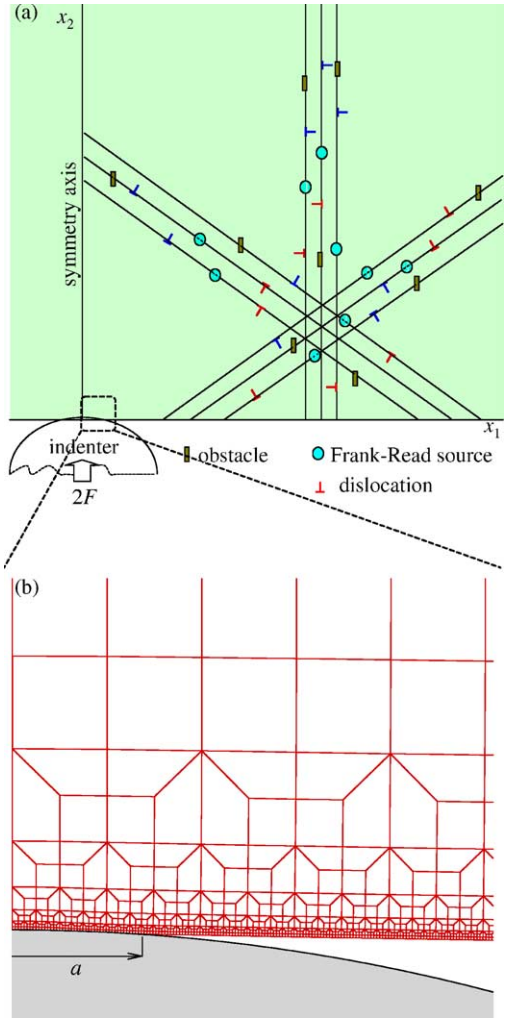

Fig. 1. (a) Model schematic: planar-symmetric crystal, with three slip systems and $x_1 = 0$ as symmetry axis. (b) Finite element mesh near indenter.

3. Results and discussion

The crystal is assumed to be elastically isotropic with Young's modulus $E = 70$ GPa and Poisson ratio $\nu = 0.33$. The magnitude of the Burgers vector is $b = 0.25$ nm and the distance between active slip planes is $100b$. Simulations are performed for various source densities, $\rho_{\text{nuc}} = 50$, 75 and 100 μm^{-2}. The strength of the sources is taken to follow a normal distribution with average strength 50 MPa and standard deviation 10 MPa. In each case the density of randomly placed obstacles, ρ_{obs}, is taken to be the same as the source density, and the obstacles have a strength of 150 MPa. The radius of the indenter is 2 μm.

Initially, the material responds elastically because no dislocations are present yet, and good agreement with the Hertz solution is obtained. As the indentation depth increases and near-indenter stresses grow large enough to generate dislocations, their motion relaxes the indentation load, Fig. 2. Oscillations in F are due to the discreteness of the dislocations. Little difference in F is found in the calculations with source densities of 75 and 100 μm^{-2} but a source density of 50 μm^{-2} gives a somewhat stiffer response.

While we track the contact length a during the simulation (Fig. 3), the hardness H is calculated using the true contact length a as $H = F/a$. The hardness curve in Fig. 4 for the lowest source density of 50 μm^{-2} shows that, beyond the elastic Hertzian regime, it gradually evolves towards a plateau value for depths above ~ 0.015 μm. For the two higher densities, $\rho_{\text{nuc}} = 75$ and 100 μm^{-2}, we see large drops in hardness, which can be traced to large jumps in contact length, shown

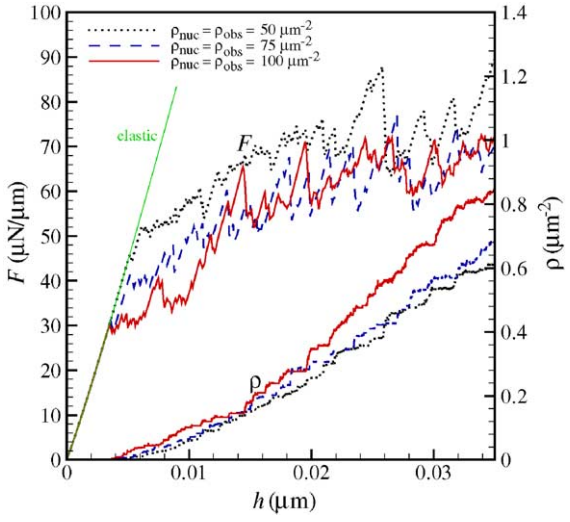

Fig. 2. Indentation load F and dislocation density ρ vs. indentation depth h for various source/obstacle densities.

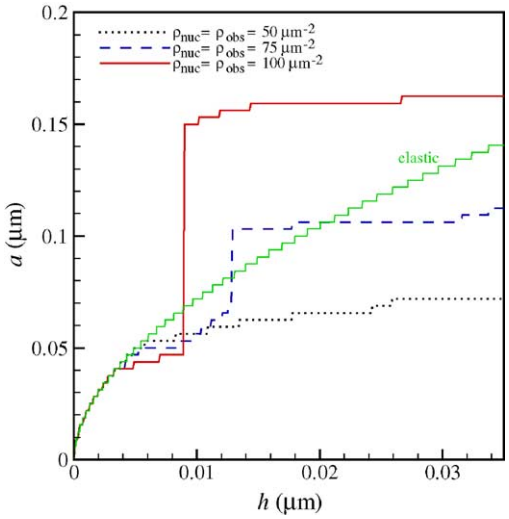

Fig. 3. Contact length a versus indentation depth h.

in Fig. 3. These jumps are due to the bursts of nucleation from a source near the surface, causing abrupt softening. After elimination of these drops, the shifted hardness curves for the two higher densities are quite close and only slightly below that for $\rho_{\text{nuc}} = 50\ \mu\text{m}^{-2}$. It should be noted that the depth at which the hardness drops sharply is likely to have some scatter since the nucleation burst is a statistical phenomenon.

The values at $h = 0.03\ \mu\text{m}$ show a clear trend of increasing hardness with decreasing source density. This is consistent with the higher dislocation density that develops with increasing source density, Fig. 2. The hardness values obtained here can be compared with the predictions of conventional non-hardening continuum plasticity, which give $H \approx 3\sigma_{\text{Y}}$ [9]. From the tension calculations in [10], it

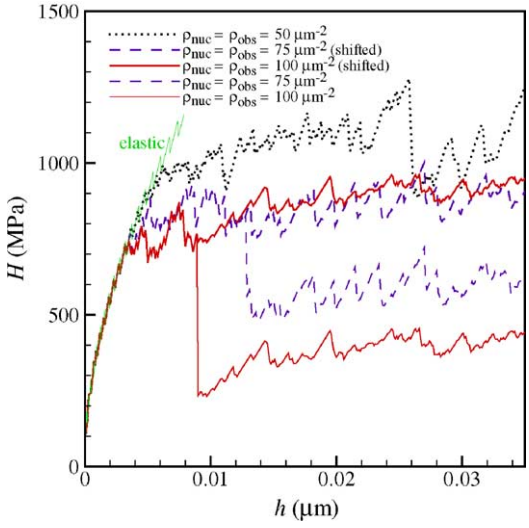

Fig. 4. Calculated hardness H versus indepentation depth h.

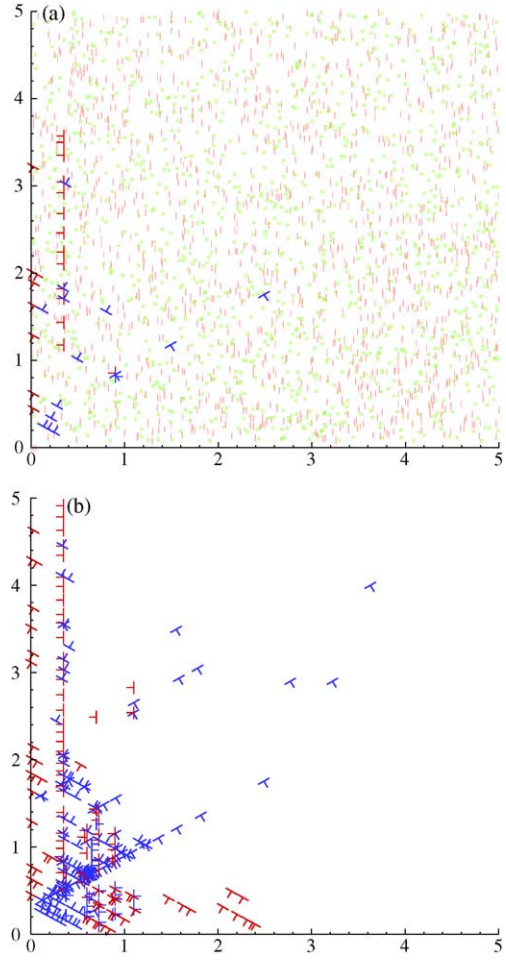

Fig. 5. Snapshots of the dislocation distribution at (a) $h = 0.01\ \mu\text{m}$ and (b) $h = 0.03\ \mu\text{m}$ for the material with $\rho_{\text{nuc}} = 50\ \mu\text{m}^{-2}$. Distances are in μm. ⊥, ○ and | symbols represent dislocation, source and obstacle, respectively.

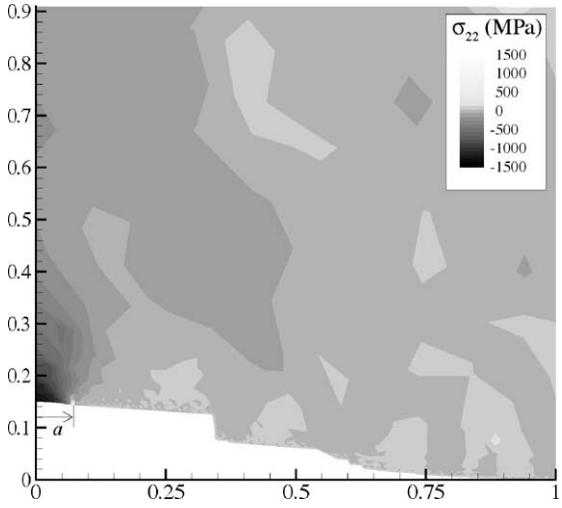

Fig. 6. Distribution of σ_{22} near the indenter tip at $h = 0.03\ \mu\text{m}$ for $\rho_{\text{nuc}} = \rho_{\text{obs}} = 50\ \mu\text{m}^{-2}$ in the deformed configuration (displacements are magnified with a factor of 5). Distances are in μm. The contact length at this stage is $a = 0.072\ \mu\text{m}$, as indicated.

is expected that the flow strength for the material parameters here is around 50 MPa, independent of source density, so that the continuum prediction is $H \approx 150$ MPa, i.e. significantly lower than our predictions even for the highest source density. We thus conclude that the availability of dislocation sources plays a strong role in setting the value of the hardness H. The reason we do not find the usual indentation size effect over the range of depths considered may be the circular shape of the indenter, see also [5].

Fig. 5 gives an impression of the dislocation structures that form for the lowest source/obstacle density analyzed. At small depths, glide mainly occurs on slip planes at 90°, i.e. parallel to the indentation direction. At larger depths, however, when more and more sources have been activated, a rather dense collection of dislocations on all slip systems develops in a region that is much larger than the depth or the contact length (Fig. 5(b)).

The stress distribution corresponding to Fig. 5(b) is shown in the deformed configuration (exaggerated for the sake of visibility) in Fig. 6. The compressive stress right above the indenter is not relaxed because of the absence of sources (the average spacing between sources is $1/\sqrt{\rho_{\text{nuc}}} \approx 0.14$ μm). Note the step in the surface profile due to localized slip on a 90° slip plane.

Acknowledgements

This research was supported by the Nederlandse Organisatie voor Wetenschappelijk Onderzoek (NWO) under project no. 635.000.007.

References

[1] M.S. De Guzman, G. Neubauer, P. Flinn, W.D. Nix, Mater. Res. Symp. Proc. 308 (1993) 613–618.
[2] Q. Ma, D.R. Clarke, J. Mater. Res. 10 (1995) 853–863.
[3] T. Zhu, J. Li, K.J. Van Vliet, S. Ogata, S. Yip, S. Suresh, J. Mech. Phys. Solids 52 (2004) 691–724.
[4] R.E. Miller, L.E. Shilkrot, W.A. Curtin, Acta Mater. 52 (2004) 271–284.
[5] H.G.M. Kreuzer, R. Pippan, Proceedings of the COMPLAS VII, Barcelona, Spain, 2003, p. 203.
[6] M. Zhao, W.S. Slaughter, M. Li, S.X. Mao, Acta Mater. 52 (2003) 4461–4469.
[7] M.C. Fivel, C.F. Robertson, G.R. Canova, L. Boulanger, Acta Mater. 46 (1998) 6183–6194.
[8] E. Van der Giessen, A. Needleman, Model. Simul. Mater. Sci. Eng. 3 (1995) 689–735.
[9] A.F. Bower, N.A. Fleck, A. Needleman, N. Ogbonna, Proc. R. Soc. Lond. A441 (1993) 97–124.
[10] V.S. Deshpande, A. Needleman, E. Van der Giessen, Acta Mater. 52 (2004) 3135–3149.